Gas separation with mixed matrix membranes obtained from MOF UiO-66-graphene oxide hybrids

Sonia Castarlenas, Carlos Téllez, Joaquín Coronas*

Department of Chemical and Environmental Engineering and Nanoscience Institute of Aragon (INA), Universidad de Zaragoza, 50018 Zaragoza, Spain.

*Corresponding author E-mail: coronas@unizar.es

Tel: +34 976 762471. Fax: +34 976 761879.

Abstract

UiO-66-GO hybrids were obtained by hydrothermal synthesis of MOF UiO-66 (a Zr terephthalate) on graphite oxide (GO). These hybrids with appropriate texture and presence of nanosized MOF particles (in the ca. 30-100 nm range) have been used as fillers to prepare mixed matrix membranes (MMMs) with two different polymers, polysulfone (PSF) and polyimide (PI), as the matrixes, with contents varying between 0 and 32 wt%. The MMMs were applied to the separation of H_2/CH_4 and CO_2/CH_4 mixtures at different temperatures (35, 60 and 90 ºC). Besides finding a good filler-polymer interaction, in the particular case of the hybrid filler, the barrier effect of the GO and the microporosity of the MOF dominated the separation properties of the MMMs. In all cases (different MMMs and separation mixtures) the effect of the temperature was to increase the permeability with a simultaneous decrease in the corresponding selectivity. In terms of permselectivity, the best H_2/CH_4 separation results were obtained (at 35 ºC) with a PI based MMM containing only UiO-66 as filler (H_2 permeability of 73 Barrer and

H_2/CH_4 selectivity of 151), while a hybrid UiO-66-GO filler produced the best CO_2/CH_4 performance (CO_2/CH_4 selectivity value of 51 at 21 Barrer of CO_2), also using a PI polymer.

Keywords: MOF, UiO-66, graphite oxide, mixed matrix membrane, polysulfone, polyimide, gas separation.

1. Introduction

Membrane technology provides greater efficiency and simplicity of operation and lower capital and operating costs than traditional separation processes such as adsorption, cryogenic distillation and low-temperature condensation [1,2]. However, it had been demonstrated that there is a limit to the performance of membrane polymers (the so called Robeson upper limit [3,4]) due to the inverse relationship between permeability and selectivity, the key parameters in gas separation with membranes. To overcome this upper bound, new materials and procedures for membrane fabrication are under investigation, particularly mixed matrix membranes (MMMs) which, by the incorporation of fillers such as zeolites [5], metal-organic frameworks (MOFs) [6,7], MOF-silicate hybrids [8], layered silicates [9] and carbon based materials [10,11], have performed better than pure polymers, approaching or even exceeding the above-mentioned Robeson limit.

Some of the most interesting filler materials for MMMs are MOFs, in which a crystalline structure is generated by linking organic ligands to metal ions [12]. Compared to traditional inorganic fillers, the interaction with the polymer is enhanced due to the organic character of the MOF linkers. In addition, the size, shape, and chemical functionalities of the MOF cavities can be tuned to some extent by choosing the appropriate linker-metal couples [13]. In this case, the MOF chosen was UiO-66, which coordinates Zr ions to terephthalic acid [14]. UiO-66 has emerged as an efficient material for CO_2 capture [15], and it has been predicted that its incorporation in a polymeric matrix would help overcome the Robeson limit in CO_2/CH_4 separation [16].

Graphite oxide (GO), prepared by chemical oxidation of graphite generating carboxylic groups, has been used to prepare a new type of hybrid material in combination with MOFs. The

new material is formed by the coordination of the metal centers with the carboxylates present in the GO structure [17,18]. MOF-GO nanocomposites combine the properties of the individual materials leading to an enhancement in ammonia adsorption in the case of MOF-5 and HKUST-1 [19], and also to the availability of new CO_2 capture and NO_2 adsorption media [20,21].

In the present study, UiO-66-GO hybrid materials were obtained by direct solvothermal synthesis of the MOF UiO-66 on previously obtained GO material. The hybrids obtained were then dispersed in the glassy polymers polysulfone and polyimide to obtain MMMs for gas separation. While several works have addressed the preparation and application of graphene oxide [22,23], UiO-66 [16,24] and MOF-GO hybrid [25-27] MMMs, there are no reports on MMMs containing the UiO-66-GO hybrid as a filler. The MMMs are used in the present study to separate H_2/CH_4 and CO_2/CH_4 mixtures, in line with two recent publications which reveal the importance of UiO-66-GO hybrids in CO_2 adsorption [28,29].

2. Experimental section

2.1. Synthesis of UiO-66-GO hybrid materials

UiO-66-GO hybrid materials were prepared by adding different amounts of graphite oxide (GO) to the typical synthesis media of UiO-66. Firstly, GO was synthesized following Hummers' method [30]. 1.5 g of sodium nitrate (+99 wt%, Acros Organics) was dissolved in 70 mL of sulfuric acid concentrate (95.0-98.0 wt%, Sigma Aldrich). Next, 3 g of graphite (RANCO 9904, 5 µm size, kindly supplied by Richard Anton KG) was added and the mixture was stirred for 30 min to obtain a homogeneous dispersion. 9 g of potassium permanganate (+99 wt%, Acros Organics) was then added gently, in an ice bath to avoid an increase in the temperature

due to the heat of the reaction. This dispersion was stirred in the ice bath for another 30 min until the formation of a viscous brown slurry. 140 mL of distilled water was added dropwise and the mixture was stirred under reflux at 95 ºC overnight. 500 mL of distilled water followed by 20 mL of hydrogen peroxide (30 wt %, Sigma Aldrich) were then added, this new mixture being maintained at 95 ºC for another 3 h under reflux. The final dispersion was filtered and washed several times with a hydrochloric acid solution and centrifuged at 10,000 rpm for 15 min until the product reached a neutral pH. The solid was then dried at 70 ºC overnight, giving rise to about 2.7 g of GO.

Following previous works [14,31], UiO-66 was synthesized with the following molar composition: 0.35 $ZrCl_4$: 5.2 CH_3COOH : 0.35 terephthalic acid : 257 DMF. Specifically, 82 mg of $ZrCl_4$ (>99.5 wt %, Sigma Aldrich) was dispersed in 0.3 mL of glacial CH_3COOH (99 wt%, Alfa Aesar) and 20 mL of DMF (> 99.5 wt%, Scharlau). This dispersion was kept in an ultrasound bath for 2 min, after which 58 mg of terephthalic acid (98wt %, Sigma Aldrich) was also added. The dispersion was transferred to a Teflon-lined autoclave and kept at 120 ºC for 24 h. The autoclave was then cooled to room temperature and the product obtained washed with ethanol and centrifuged at 10,000 rpm for 15 min twice. The resulting solid was activated with methanol at 80 ºC for 48 h, centrifuged again under the conditions described above and dried at 80 ºC for 24 h to obtain about 65 mg of activated UiO-66.

To prepare the UiO-66-GO hybrid materials, different amounts of GO (20 and 30 mg) were added to the synthesis media above described for UiO-66. The syntheses took place at 120 ºC for 24, 48 and 72 h, following the same purification-activation procedure used for UiO-66. Table 1 shows complementary information about the different hybrids produced.

2.2. Preparation of Mixed Matrix Membranes (MMMs)

GO, UiO-66 and some selected UiO-66-GO hybrid materials were used as fillers for flat MMMs for which polysulfone (PSF, Udel® 3500-P kindly supplied by Solvay Advanced Polymers) and polyimide (PI, Matrimid® kindly supplied by Huntsman) were used as polymeric matrixes. The preparation of these MMMs consisted of the dispersion of the filler in chloroform, after which the corresponding polymer was added [8]. The solvent/filler-polymer proportion was 90/10 wt% and the final filler loading of the MMMs was between 0-32 wt%. The whole mixture was magnetically stirred overnight and treated in an ultrasonic bath for 15 min. Subsequently, the membranes were cast on a Petri dish, and then left overnight for natural evaporation of the chloroform at room temperature. Once dried, the films were placed for the same period of time under 10 mbar pressure in a Memmert VO 200 vacuum oven to remove the remaining solvent at 120 ºC in the case of PSF membranes and at 180 ºC in the case of PI membranes. Thicknesses of 50 ± 10 µm were measured using a micrometer (accuracy of 0.001 mm, Mitutoyo Corp.). To compare all the results, besides GO, UiO-66 and UiO-66-GO, a physical mixture of GO and UiO-66 in a 1:1 weight ratio was also used as filler. The membranes were named MMM_Pol_Filler_Percentage, where Pol represents the specific polymer, Filler is the additive and Percentage is the wt% content of the filler in the final membrane.

2.3. Characterization

All the materials and the membranes were characterized by X-ray diffraction (XRD) using a D-Max Rigaku X-ray diffractometer with a copper anode and a graphite monochromator to select CuKα radiation (λ=1.5418Å) from 5º to 40 º (2θ) with a 0.038º/s step.

Nitrogen adsorption-desorption isotherms of UiO-66-GO hybrid materials were measured at -196 ºC using a porosity analyzer (TriStar 3000, Micromeritics Instrument Corp.). The samples were outgassed with a heating rate of 10 °C/min until 250 ºC and maintained for 8 h.

Thermogravimetric analyses (TGA) were performed using a Mettler Toledo TGA/SDTA 851e system. Samples (10 mg) placed in 70 µL alumina pans were heated in N_2 flow up to 850 °C at a heating rate of 10 ^{o}C/min.

Differential scanning calorimetry (DSC) of the membranes was measured using Mettler Toledo DSC822 equipment. The glass transition temperature was calculated mathematically as the inflection point of the transition region in the second and the third heating cycle and using the average value. For each filler loading, three different membrane samples were measured.

Scanning electron microscopy (SEM) images were collected with an Inspect F scanning electron microscope to evaluate the size of the particles and the dispersion of the filler through the membrane, and the contact between the filler and the polymeric phase. Cross sections were prepared by freeze-fracturing after immersion in liquid N_2 and subsequent 15 nm gold coating.

2.4. Gas separation

Circular 15.2 cm^2 membranes were analyzed for H_2/CH_4 and CO_2/CH_4 separations. The permeation module consisted of two stainless steel pieces with a cavity in which the membrane was placed and a macroporous disk support 316LSS of 20 µm nominal pore size (Mott Corp.) gripped inside with Viton O-rings. Mass-flow controllers (MC-100SCCM-D, Alicat Scientific) fed a 25/25 cm^3(STP)/min stream of the gas mixture to the retentate side of the membrane at 340 kPa, while the permeate side of the membrane was swept with a 1 cm^3(STP)/min stream of an inert gas (Ar or He depending on the gas mixture) at atmospheric pressure. Concentrations in the

outgoing streams were analyzed by an Agilent 3000A online gas microchromatograph equipped with a TCD. Permeability results in Barrer (1 Barrer= $1 \cdot 10^{-10}$ cm^3 (STP)·cm/(cm^2·s·cmHg)) were obtained once the permeate stream was stabilized (after about 2 h under stream). The gas pair selectivity was calculated as the ratio of permeability values. The permeation measurements were performed at 35, 60 and 90 ºC, controlled by a Memmert UNE 200 oven. Available errors for permeability and selectivity values were calculated for 3-5 different membranes tested under the same conditions.

3. Results and discussion

3.1. UiO-66-GO hybrid materials

Table 1 shows relevant characteristics of the GO, UiO-66 and UiO-66-GO hybrid materials. The UiO-66 wt% values in the final sample were obtained by drying the product at the end of the synthesis and considering that GO (constituted initially by both large, up to 10 μm thick agglomerates and fine particles as thin as 15 nm, as observed by SEM and TEM, not shown) was not dissolved during the solvothermal crystallization in DMF. Figure 1 depicts the SEM characterization of the hybrids. These images and that corresponding to UiO-66 alone (Figure S1) allowed the particle size analysis corresponding to the cumulative particle size distributions in Figure S2. Average particle sizes (Table 1) were obtained at N/N_T 0.5 (N and N_T being the normalized number and total number of particles, respectively). From these average particle sizes, it can be inferred that in the absence of GO in the synthesis media, the size of the UiO-66 particles was larger than when GO was present for the same synthesis time (e.g. at 24 h synthesis time, 87 nm for pure UiO-66 and 29 and 36 nm when 20 and 30 mg of GO were

present in the synthesis media, respectively). Besides, for the same amount of GO present in the synthesis, the particle size increased with synthesis time. The amount of GO also affected the particle size, this is more evident at high synthesis times of 48 and 72 h. All these findings suggest that GO affects the nucleation rate of the MOF, and the larger amount of GO (30 mg) would generate some worse crystallinity consistent with a higher nucleation rate (due to the presence of more nucleation sites in the synthesis medium) giving rise to larger particles by aggregation. In fact, the content of UiO-66 in the samples is similar (54-59 wt%), independently of the amount of GO used, in agreement with a higher MOF synthesis yield with 20 mg GO (ca. 38 mg MOF) than with 30 mg GO (ca. 38 mg MOF).

Table 1. Synthesis conditions and textural properties of GO, UiO-66 and GO@UiO-66 hybrid materials. S_{BET} and S_{EXT} refer to BET and external specific surface areas, respectively

Sample	**GO [mg]**	**Synthesis time [h]**	**UiO-66 [wt%]**	**UiO-66 size [nm]**	**S_{BET} [m^2/g]**	**S_{EXT} [m^2/g]**
GO	-	-	0	-	25	25
UiO-66	0	24	100	87	1342	130
GO(20)_UiO-66_24h	20	24	57	29	833	136
GO(20)_UiO-66_48h	20	48	58	49	842	176
GO(20)_UiO-66_72h	20	72	59	55	851	135
GO(30)_UiO-66_24h	30	24	54	36	614	127
GO(30)_UiO-66_48h	30	48	57	87	665	176
GO(30)_UiO-66_72h	30	72	57	102	703	136

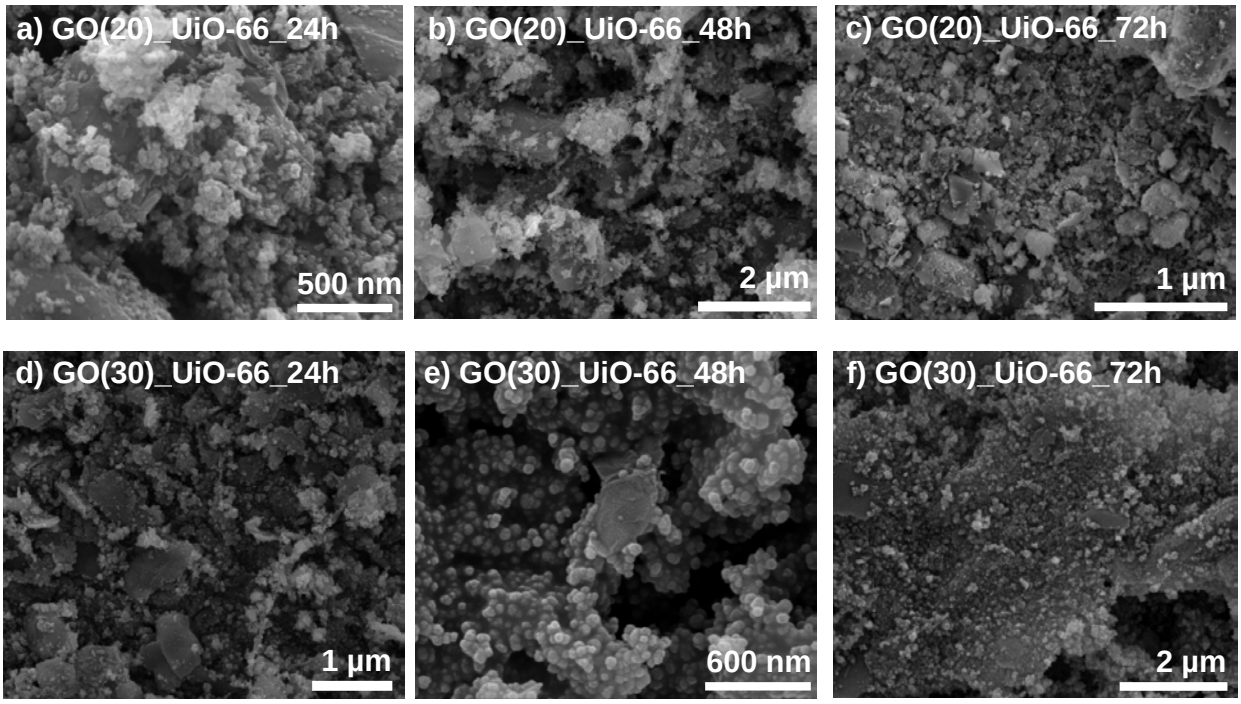

Figure 1. SEM images of the different GO@UiO-66 hybrids prepared with different amounts of GO at different synthesis times.

X-ray diffraction patterns of the parent GO and UiO-66 and the hybrid materials (Figure 2) provide information about their structures. The characteristic peak of GO appears at 2·theta 12º, corresponding, according to Bragg's Law, to an interlayer spacing of 0.74 nm [32]. All the hybrids show the typical peaks of UiO-66, mainly those corresponding to (111) and (002) crystallographic planes at 7.2º and 8.0º, respectively [14]. In the hybrids, the GO peak is scarcely observed. This may be due to a better dispersion or even to some exfoliation of the GO layers during the synthesis helped by the intercalation of MOF nanoparticles between GO sheets. In addition, the solvent used is DMF which has previously been used to perform this exfoliation [33,34]. It may also be due to the fact that in the hybrids the intensities of the more crystalline UiO-66 predominated over those of the less crystalline GO, making the UiO-66 peaks more

visible. Comparing the results of the different hybrid materials, it can be observed that the peaks are broader when the synthesis time is shorter. This may be due to the smaller size of the particles (see Table 1).

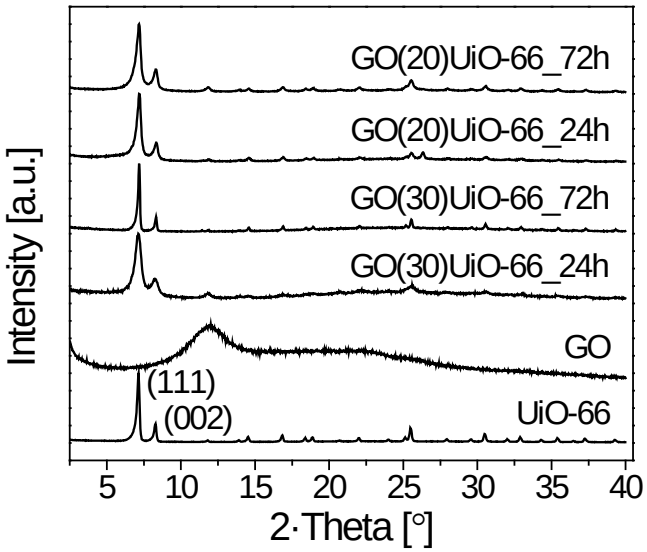

Figure 2. X-ray diffraction patterns of UiO-66, GO and the hybrid materials GO(20)_UiO-66_24h, GO(20)_UiO-66_72h, GO(30)_UiO-66_24h and GO(30)_UiO-66_72h.

Table 1 shows the BET (S_{BET}) and external (S_{EXT}) specific surface area values of GO, UiO-66 and GO@UiO-66 hybrid materials calculated by the t-plot method. GO with only 25 m^2/g of BET specific surface area is considered as nonporous since its surface is inaccessible to N_2 molecules [32]. The incorporation of GO decreases both the BET and microporous specific surface areas as compared to the values of MOF UiO-66 (1342 and 1212 m^2/g, respectively) and the microporous area. The reduction of the BET specific surface area has also been observed in MOF-5-GO hybrids [18], but this reduction was in a smaller proportion due to a smaller GO

content (in that case the materials had 5 wt% of GO). Moreover, the decrease in the microporous area follows a similar trend. By increasing the amount of GO from 20 (S_{BET} 833-851 m^2/g) to 30 mg (S_{BET} 614-703 m^2/g), both the BET and microporous specific surface areas decreased and a longer synthesis time was needed to compensate for such decreases. This suggests that GO may exert some influence on the nucleation and crystal growth of the MOF, in agreement with the previous discussion dealing with particle size and crystallinity. If a higher sample microporosity is related to a higher crystallinity of the MOF, this parameter decreases with the amount of GO and increases with synthesis time. It is worth mentioning that a previously reported GO-UiO-66 hybrid (with 1-10 wt% of GO added in the MOF synthesis) gave BET specific surface area values of 923-1184 m^2/g [28].

To study the interaction between GO and MOF UiO-66, TGA curves and their derivatives are shown in Figure 3 for the amounts of GO present in the synthesis media. In the case of UiO-66, three stages can be observed related to surface water evaporation (<100 ºC), DMF residue (150-300 ºC) and collapse of the structure (480-575 ºC), where the final residue is considered to be ZrO_2. The GO curve presents four decomposition stages related to the removal of physically adsorbed water (<100 ºC), the decomposition of epoxy groups (150-200 ºC), and the decomposition of carboxylic groups (250-450 ºC) [32]. The last of the weight losses (>500 ºC) is due to the decomposition of the carbonaceous remains. The intermediate decomposition stages of both materials, GO and UiO-66, can be observed in the hybrids, while they overlap in the final decomposition stage. An increase in the temperature of the final decomposition stage may be deduced as a function of the synthesis time of the MOF. This may be due to the fact that by increasing the synthesis time, the particle size also increased, thus diffusion of the air and the decomposition products may have been impeded. Figure S3 shows the influence of the amount

of GO for the same synthesis time. In this case, it can be observed how the final decomposition stage is more similar to that of pure UiO-66 when a smaller amount of GO was present. It can also be seen how the proportion of GO in the hybrid increased by increasing the initial amount of GO present in the synthesis media. On the other hand, the proportion of GO in the final hybrid decreased as the synthesis time increased. Finally, UiO-66-GO materials GO(30)_UiO-66_48h and GO(30)_UiO-66_72h were chosen as fillers for mixed matrix membranes with both polysulfone (PSF) and polyimide (PI) polymers. These two fillers will serve to illustrate the combined effect of both GO barrier and MOF microporosity effects in the same MMM. UiO-66-GO hybrids obtained from 30 mg of GO at 48 h and 72 h were chosen because of the particle size between 80 and 100 nm which would reduce possible particle agglomeration during MMMs preparation.

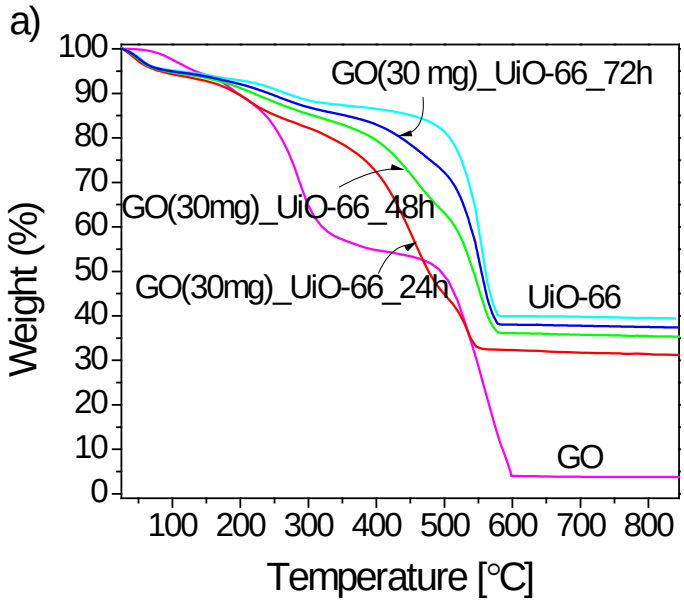

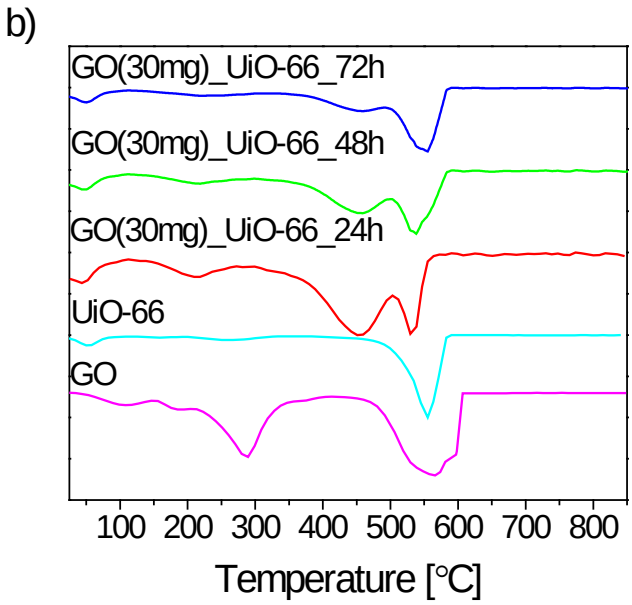

Figure 3. a) TGA curves of GO, UiO-66, GO(30)_UiO-66_24h, GO(30)_UiO-66_48h, GO(30)_UiO-66_72h; b) their derivative curves.

3.2. Characterization of MMMs

MMMs combining GO(30)_UiO-66_48h and GO(30)_UiO-66_72h as fillers and PI or PSF as polymers were prepared with loadings from 0 to 32 wt %. To study the influence of GO on the permselective properties, MMMs containing GO and UiO-66 as fillers were also prepared. Moreover, to ensure that the observed effects were related to the interaction between both materials, MMMs with a blend of GO and UiO-66 in a proportion of 1:1 were also prepared. In addition to the SEM images suggesting good filler-polymer interaction and homogeneous dispersion (Figure S4), X-ray diffraction was also carried out to observe the interaction between the UiO-66-GO hybrids and the corresponding polymer and to ensure that the UiO-66 structure was not lost. Figures 4a and 4b show the results for PI and PSF based MMMs, respectively.

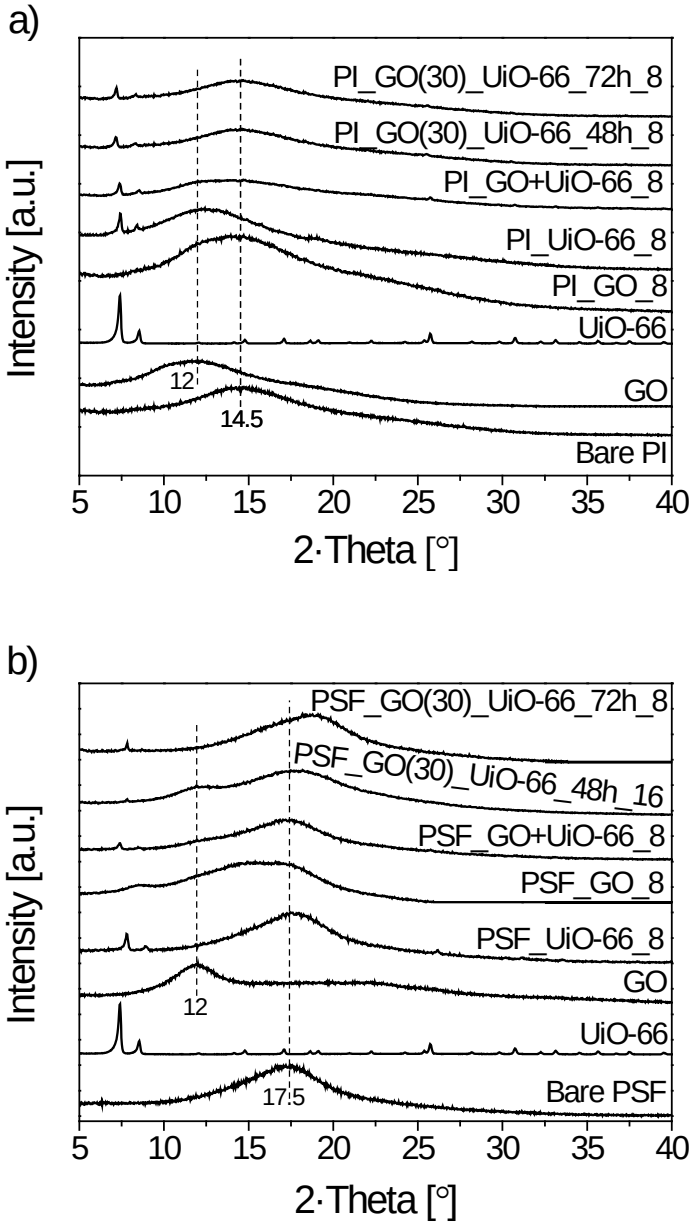

Figure 4. XRD patterns of MMMs: a) based on PI, b) based on PSF.

When PI is the matrix and GO the filler, it can be observed how the GO characteristic peak, which usually appears at 2·theta ca. 12º, does not appear clearly in the MMM and the peak corresponding to the polymer seems to be broader. For this same filler, when PSF is the matrix, it

can be observed how the GO peak shifts to 2·theta ca. 8.5º, producing a variation of the interlayer spacing in GO from 0.74 nm to 1.0 nm. This suggests that the interaction between GO and PSF may help to produce a partial exfoliation of the GO layers. This effect was also observed in membranes whose matrix was polyethylene oxide where the GO peak shifted to 2·theta 4.5º [35]. The characteristic peak of PSF becomes broader and shifts from 2·theta 17.5º to about 16º (the interlayer spacing changes from 0.51 nm to 0.56 nm), which is consistent with the interpenetration between GO layers and PSF polymer chains. When UiO-66 is the filler, whether or not blended with GO, the (111) and (002) characteristic peaks are also observed in the MMMs while the PSF peak remains constant at the value corresponding to the bare polymer, i.e. to an interlayer spacing of 0.51 nm. In the case of the MMMs containing the hybrid materials, the polymer peak moves to high values of 2·theta (up to 18.7º, 0.48 nm) in agreement with a stronger filler-polymer interaction, as observed in other filler-PSF MMMs [36,37]. It is worth mentioning that this positive result (positive from the point of view of the filler-polymer interaction) was only achieved with PSF and with the hybrids, where the MOF-polymer interaction is favored through the availability of well dispersed small MOF nanoparticles (supported on GO sheets) with higher specific surface area. It was not achieved with PI, whose polymer chains are about 0.1 nm wider than those of PSF, in agreement with the respective diffraction peaks at 14.5º (0.61 nm) and 17.5º (0.51 nm).

DSC analyses were carried out to calculate the glass transition temperatures (T_g) of the polymers. Table S1 shows some increase in the T_g values between the pure polymers (183 ºC and 317 ºC for PSF and PI, respectively) and the MMMs containing only GO (187 ºC and 320 ºC for PSF and PI, respectively) and a further increase in the case of the MMMs with either the MOF or the hybrids (191-195 ºC and 331-337 ºC for PSF and PI, respectively). This indicates some

increasing rigidification due to the filler-polymer interaction but there are no significant differences between the MOF and the MOF-GO hybrids. It can be inferred from these results that the influence of the MOF covering the GO surface predominates in the filler-polymer interaction in terms of T_g changes. It is worth mentioning that in the case of the GO-containing MMMs, the loading of the filler (8 wt%) is much lower than in the other cases (32 wt%).

3.3. Gas separation results

All the MMMs were tested in gas separation experiments with H_2/CH_4 and CO_2/CH_4 mixtures. The effect of the temperature was also studied by measuring the separation performance at 35, 60 and 90 ºC.

In the case of the H_2/CH_4 separation, the strong barrier effect of GO was observed. An increase in the amount of this filler produced a significant decrease in the H_2 permeability and the selectivity (Figure S5). The loss of separation selectivity can be related to the difficult of obtaining good dispersion of GO in a given polymer, something that would be corrected, from the point of view of the MMM separation performance, when using the MOF containing hybrids. This behavior was observed for both PSF and PI polymers and both mixtures, H_2/CH_4 and CO_2/CH_4 (Figures S5 and S6). The rest of the fillers showed the opposite behavior. In all cases (UiO-66, the GO_UiO-66 hybrids and the GO + UiO-66 physical mixture) both the permeability and selectivity increased when the amount of the filler was increased, reaching a maximum selectivity value. This can be more clearly observed in the selectivity versus permeability plots (Figure 5). It can be noted that in the case of the H_2/CH_4 separation (mainly based on differences in diffusion, H_2 and CH_4 having kinetic diameters of 0.29 nm and 0.38 nm, respectively), the MMMs closest to the upper bound are those prepared with only UiO-66 and PI as the polymer.

In these cases the H_2/CH_4 separation was not penalized, showing the maximum value (151), while the H_2 permeability was the highest (75 Barrer) due to the absence of the GO barrier effect present to some extent in the hybrids. Regarding the CO_2/CH_4 separation, the results were again better with PI than PSF. In addition, there was a clear enhancement of both permeability and selectivity with MOF loading for both UiO-66 and the UiO-66-GO hybrids. However, unlike the previous H_2/CH_4 mixture, the selectivity as a function of the CO_2 permeability passed through a clear maximum that corresponds to a CO_2/CH_4 selectivity value of 51 at 21 Barrer of CO_2. This was achieved with the MMMs obtained with the hybrid GO(30)_UiO-66_48h and the PI polymer at 24 wt% filler loading. Indeed, this hybrid has the highest external surface area (Table 1). Finally, note that in all cases (different polymers and separation mixtures) the MMMs obtained with the blending of UiO-66 and GO fillers performed worse (in the best case lower permeability with similar selectivity) than those prepared with the hybrid materials. This demonstrates that: i) the hybrid materials have a lesser barrier effect than GO, perhaps due to exfoliation of the GO and the creation of defects in its layers during the preparation and activation of the MOF, ii) the filler-polymer interaction is improved in these composites, and iii) the transport properties of the membranes are enhanced because of the microporosity properties of the MOF. The latter is of particular importance in the case of the CO_2/CH_4 separation where the selectivity increased with the permeability, passing through a maximum, when the filler content was augmented (see Figure 5b). Both CO_2 diffusion (the CO_2 and CH_4 kinetic diameters are 0.33 nm and 0.38 nm, respectively) and adsorption were favored with the efficient action of the MOF well dispersed due to its synthesis on the GO sheets [28,29].

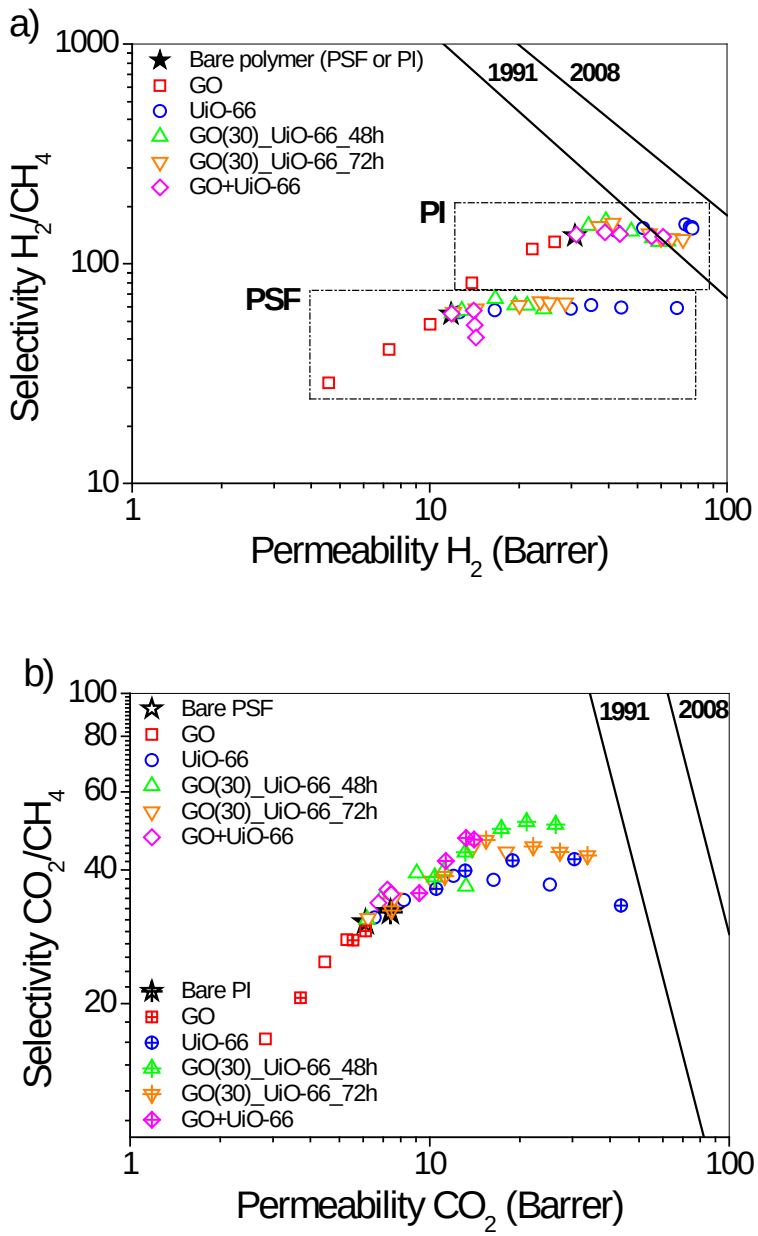

Figure 5. a) H_2/CH_4 selectivity as a function of H_2 permeability. b) CO_2/CH_4 selectivity as a function of CO_2 permeability. In both cases 1991 and 2008 Robeson upper limits [3,4] are plotted for comparison.

To study the influence of the temperature (in the 35-90 ºC range) on the H_2, CO_2 and CH_4 permeabilities with both polymers, PSF and PI, and in both H_2/CH_4 and CO_2/CH_4 mixtures,

some selected membrane samples prepared at certain filler contents (those showing the highest selectivity values in Figures S5 and S6) were analyzed with the Arrhenius equation:

$$P_i = P_{0,i} \cdot e^{\left(-\frac{E_{ap}}{RT}\right)} \qquad \text{Eq. 1}$$

where P_i is the permeability of the gas, $P_{0,i}$ is the pre-exponential factor with the same units as the permeability (Barrer), R is the universal gas constant (8.314 J/mol·K), T is the absolute temperature (K) and E_{ap} the apparent activation energy (J/mol). The simple idea behind these experiments was to increase the permeability while keeping a high level of separation selectivity. Figures 6a and 6b show, for the two mixtures, systematic decreases in selectivity as a function of permeability, when the latter was augmented by the effect of the temperature. In this situation, the permeability-selectivity lines run parallel to the upper bound limits. Moreover, the behavior of E_{ap} of the gases is typically governed by molecular sieving and interaction with the polymer (solubility). As shown in Table S2, gases with low E_{ap} values (H_2 and CO_2 as compared with CH_4) exhibit a high permeability, in agreement with previous analogous studies [38]. This fact explains the decreases observed in both H_2/CH_4 and CO_2/CH_4 selectivities as a function of temperature. Finally, with the exception of the GO MMMs, the other types of MMMs (with UiO-66 and the UiO-66-GO hybrid) present slightly higher activation energies than the bare polymer membranes for all three gases. This is consistent with an enhancement of the transport through the microporosity of the MOF-containing MMMs.

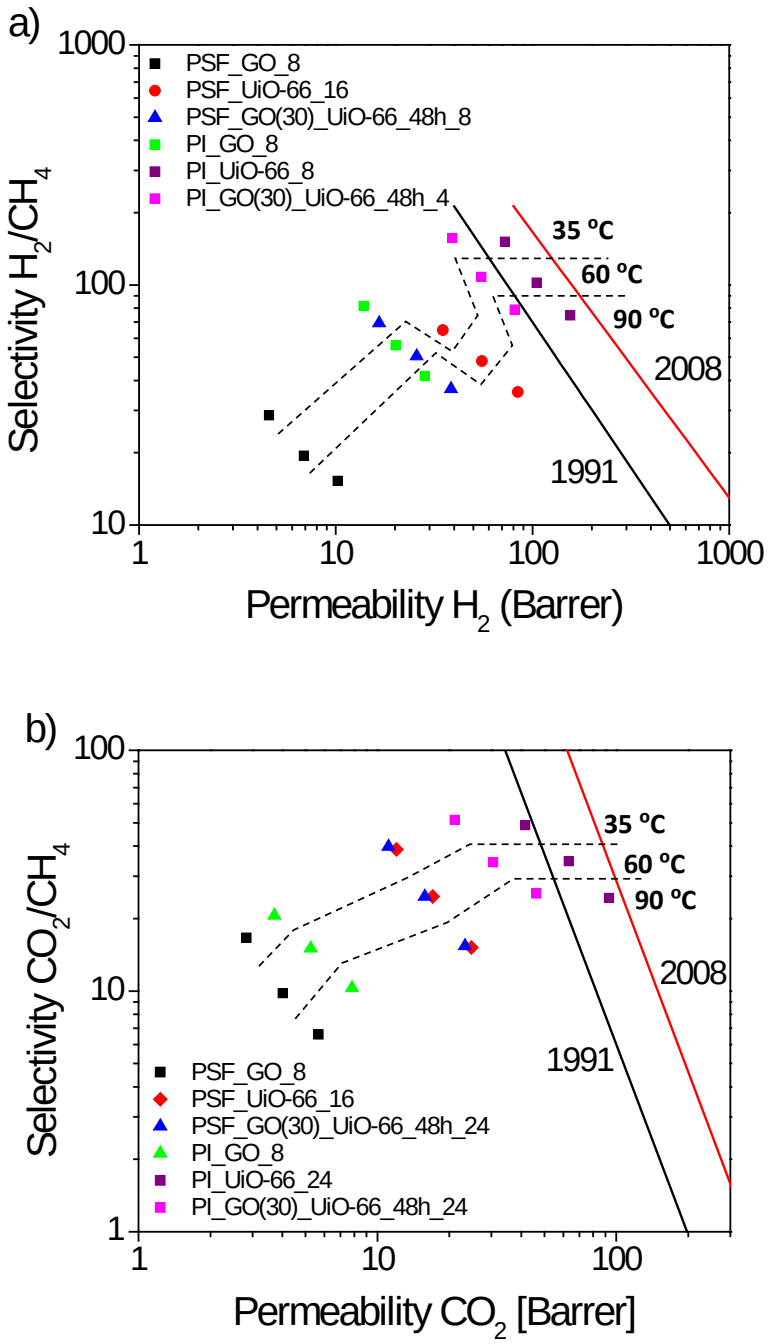

Figure 6. Separation results for the most important MMMs at 35, 60 and 90 ºC: a) H_2/CH_4, b) CO_2/CH_4. In both cases 1991 and 2008 Robeson upper limits [3,4] are plotted for comparison. Dashed lines separate results obtained at different temperatures.

Conclusions

The hydrothermal synthesis of MOF UiO-66 on GO sheets produced hybrid materials showing SEM, XRD and porosity features of both GO and UiO-66 materials. Moreover, the hybrids exhibit both high BET and external specific surface areas and the presence of nanosized particles of UiO-66. These two properties are of great important for producing MMMs with enhanced filler-polymer interaction and where the crystalline nature of UiO-66 is preserved, as shown by XRD. In fact, the XRD characterization showed clearer effects (shifts to high 2·theta values due to filler-polymer chain interactions) on polysulfone than on polyimide. In addition, it was evidenced that the mere UiO-66 and GO blending was less effective than the UiO-66-GO hybrid.

Regarding membrane performance, a strong barrier effect of GO was observed producing significant decreases in the H_2 and CO_2 permeabilities for MMMs with both PSF and PI polymers and for both mixtures, H_2/CH_4 and CO_2/CH_4. The presence of UiO-66 compensated for the barrier effect in the MMMs prepared with the hybrids. However, this effect was still significant for the H_2/CH_4 mixture (whose separation is mainly based on differences in kinetic diameters), and the best H_2/CH_4 separation results in terms of both permeability and selectivity were obtained with a PI based MMM containing only UiO-66 as filler. In the case of the CO_2/CH_4 separation, where both CO_2 diffusion and adsorption are favored with the efficient action of the MOF well dispersed on the GO sheets, the UiO-GO hybrids gave rise to the best separation results.

Acknowledgements

Financial support from Obra Social la Caixa and the Aragón Government (T05 and GA-LC-019/2011), and the ESF is gratefully acknowledged. We also acknowledge the use of the

Servicio General de Apoyo a la Investigación-SAI (Universidad de Zaragoza). All the microscopy work was done in the Laboratorio de Microscopías Avanzadas at the Instituto de Nanociencia de Aragón (LMA-INA). The authors acknowledge the LMA-INA for offering access to their instruments and expertise.

References

1. R.W. Baker, Future Directions of Membrane Gas Separation Technology, Ind. Eng. Chem. Res. 41 (2002) 41 1393-1411.

2. R. Mahajan, W.J. Koros, Factors Controlling Successful Formation of Mixed-Matrix Gas Separation Materials, Ind. Eng. Chem. Res. 39 (2000) 2692-2696.

3. L.M. Robeson, Correlation of separation factor versus permeability for polymeric membranes, J. Membr. Sci. 62 (1991) 165-185.

4. L.M. Robeson, The upper bound revisited, J. Membr. Sci. 320 (2008) 390-400.

5. V. Martin-Gil, A. López, P. Hrabanek, R. Mallada, I.F.J. Vankelecom, V. Fila, Study of different titanosilicate (TS-1 and ETS-10) as fillers for Mixed Matrix Membranes for CO2/CH4 gas separation applications, J. Membr. Sci. 523 (2017) 24-35.

6. B. Zornoza, C. Tellez, J. Coronas, J. Gascon, F. Kapteijn, Metal organic framework based mixed matrix membranes: An increasingly important field of research with a large application potential, Microporous Mesoporous Mater. 166 (2013) 67-78.

7. M.W. Anjum, F. Vermoortele, A.L. Khan, B. Bueken, D.E. De Vos, I.F.J. Vankelecom, Modulated UiO-66-based mixed-matrix membranes for CO2 separation, ACS Appl. Mater. Interfaces 7 (2015) 25193−25201.

8. S. Sorribas, B. Zornoza, C. Téllez, J. Coronas, Mixed matrix membranes comprising silica-(ZIF-8) core–shell spheres with ordered meso–microporosity for natural- and bio-gas upgrading, J. Membr. Sci. 452 (2014) 184-192.

9. C. Rubio, B. Zornoza, P. Gorgojo, C. Tellez, J. Coronas, Separation of H2 and CO2 containing mixtures with mixed matrix membranes based on layered materials, Curr. Org. Chem. 18 (2014) 2351-2363.

10. C.M. Zimmerman, A. Singh, W.J. Koros,Tailoring mixed matrix composite membranes for gas separations, J. Membr. Sci. 137 (1997) 145-154.

11. Y. Shin, E. Prestat, K.-G. Zhou, P. Gorgojo, K. Althumayri, W. Harrison, P.M. Budd, S.J. Haigh, C. Casiraghi, Synthesis and characterization of composite membranes made of graphene and polymers of intrinsic microporosity, Carbon 102 (2016) 357-366.

12. O.M. Yaghi, M. O'Keeffe1, N.W. Ockwig, H.K. Chae, M. Eddaoudi, J. Kim synthesis and the design of new materials. Nature 423 (2003) 705-714.

13. R. Banerjee, H. Furukawa, D. Britt, C. Knobler, M. O'Keeffe, O.M. Yaghi, Control of pore size and functionality in isoreticular zeolitic imidazolate frameworks and their carbon dioxide selective capture properties. J. Am. Chem. Soc. 131 (2009), 3875-3877.

14. J. H. Cavka, S. Jakobsen, U. Olsbye, N. Guillou, C. Lamberti, S. Bordiga, K.P. Lillerud, A new zirconium inorganic building brick forming metal organic frameworks with exceptional stability, J. Am. Chem. Soc. 130 (2008) 13850-13851.

15. Y. Huang, W. Qin, Z. Li, Y. Li, Enhanced stability and CO2 affinity of a UiO-66 type metal-organic framework decorated with dimethyl groups, Dalton Trans. 41 (2012) 9283-9285.

16. D. Wu, G. Maurin, Q. Yang, C. Serre, H. Jobic, C. Zhong, Computational exploration of a Zr-carboxylate based metal-organic framework as a membrane material for CO2 capture, J. Mater. Chem. A 2 (2014) 1657-1661.

17. C. Petit, T.J. Bandosz, MOF-graphite oxide composites: combining the uniqueness of graphene layers and metal-organic frameworks, Adv. Mater. 21 (2009) 4753-4757.

18. C. Petit, T.J. Bandosz, MOF-graphite oxide nanocomposites: surface characterization and evaluation as adsorbents of ammonia, J. Mater. Chem. 19 (2009) 6521-6528.

19.T.J. Bandosz, C. Petit, MOF/graphite oxide hybrid materials: exploring the new concept of adsorbents and catalysts, Adsorption 17 (2010) 5-16.

20. A. Policicchio, Y. Zhao, Q. Zhong, R.G. Agostino, T.J. Bandosz, Cu-BTC/aminated graphite oxide composites as high-efficiency CO2 capture media, ACS Appl. Mater. interfaces 6 (2013) 101-108.

21. A.M. Ebrahim, B. Levasseur, T.J. Bandosz, Interactions of NO2 with Zr-based MOF: effects of the size of organic linkers on NO2 adsorption at ambient conditions, Langmuir 29 (2012) 168-174.

22. B.M. Ganesh, A..M Isloor, A.F. Ismail, Enhanced hydrophilicity and salt rejection study of graphene oxide-polysulfone mixed matrix membrane, Desalination 313 (2013) 199-207.

23. S. Zinadinia, A.A. Zinatizadeha, M. Rahimib, V. Vatanpourc, H. Zangeneh, Preparation of a novel antifouling mixed matrix PES membrane by embedding graphene oxide nanoplates, J. Membr. Sci. 453 (2014) 292-301.

24. M.W. Anjum, F. Vermoortele, A.L. Khan, B. Bueken, D.E. De Vos, I.F.J. Vankelecom, Modulated UiO-66-based mixed-matrix membranes for CO2 separation, ACS Appl. Mater. Interfaces 45 (2015) 25193-25201.

25. M. Sarfraz, M. Ba-Shammakh, Synergistic effect of incorporating ZIF-302 and graphene oxide to polysulfone to develop highly selective mixed-matrix membranes for carbon dioxide separation from wet post-combustion flue gases, J. Ind. Eng. Chem. 36 (2016)154-162.

26. M. Sarfraz, M. Ba-Shammakh, Synergistic effect of adding graphene oxide and ZIF-301 to polysulfone to develop high performance mixed matrix membranes for selective carbon dioxide separation from post combustion flue gas, J. Membr. Sci. 514 (2016) 35-43.

27. L. Dong, M. Chen, J. Li, D. Shi, W. Dong, X. Li, Y. Bai, Metal-organic framework-graphene oxide composites: A facile method to highly improve the CO2 separation performance of mixed matrix membranes, J. Membr. Sci. 520 (2016) 801-811.

28. Y. Cao, Y. Zhao, Z. Lv, F. Song, Q. Zhong, Preparation and enhanced CO2 adsorption capacity of UiO-66/graphene oxide composites, J. Ind. Eng. Chem. 27 (2015) 102–107.

29. A.R. Noorpoor, S.N. Kudahi, Analysis and study of CO2 adsorption on UiO-66/graphene oxide composite using equilibrium modeling and ideal adsorption solution theory (IAST), J. Environ. Chem. Eng. 2 (2016) 1081–1091.

30. W.S. Hummers, R.E. Offeman, Preparation of graphitic oxide, J. Am. Chem. Soc. 80 (1958) 1339-1339.

31. H.R. Abid, H. Tian, H.M. Ang, M.O. Tade, C.E: Buckley, S. Wang, Nanosize Zr-metal organic framework (UiO-66) for hydrogen and carbon dioxide storage, Chem. Eng. J. 187 (2012) 415-420.

32. M. Seredych, C. Petit, A.V. Tamashausky, T.J. Bandosz, Role of graphite precursor in the performance of graphite oxides as ammonia adsorbents, Carbon 47 (2009) 47 445-456.

33. Y. Hernandez, V. Nicolosi, M. Lotya, F.M. Blighe, Z. Sun, S. De, I.T: McGovern, B. Holland, M. Byrne, Y.K. Gun'Ko, J.J. Boland, P. Niraj, G. Duesberg, S. Krishnamurthy, R.

Goodhue, J. Hutchison, V. Scardaci, A.C. Ferrari, J.N. Coleman, High-yield production of graphene by liquid-phase exfoliation of graphite, Nat. Nanotechnol. 3 (2008) 563-568.

34. C.J. Shih, S. Lin, M.S. Strano, D. Blankschtein, Understanding the stabilization of liquid-phase-exfoliated graphene in polar solvents: molecular dynamics simulations and kinetic theory of colloid aggregation, J. Am. Chem. Soc. 132 (2010) 14638-14648.

35. Y.C. Cao, C. Xu, X. Wu, X. Wang, L. Xing, K. Scott, A poly (ethylene oxide)/graphene oxide electrolyte membrane for low temperature polymer fuel cells. J. Power Sources 196 (2011) 8377-8382.

36. F. Li, Y. Li, T.S. Chung, S. Kawi, Facilitated transport by hybrid POSS®–Matrimid®–Zn2+ nanocomposite membranes for the separation of natural gas, J. Membr. Sci. 356 (2010) 14–21.

37. B Zornoza, C Tellez, J Coronas, Mixed matrix membranes comprising glassy polymers and dispersed mesoporous silica spheres for gas separation, J. Membr. Sci. 368 (2011) 100-109.

38. R. Pal, Permeation models for mixed matrix membranes, J. Colloid Interface Sci. 317 (2008) 191-198.

Supporting information

Gas separation with mixed matrix membranes obtained from MOF UiO-66-graphene oxide hybrids

Sonia Castarlenas, Carlos Téllez, Joaquín Coronas*

Department of Chemical and Environmental Engineering and Nanoscience Institute of Aragon (INA), Universidad de Zaragoza, 50018 Zaragoza, Spain.

*Corresponding author E-mail: coronas@unizar.es

Tel: +34 976 762471. Fax: +34 976 761879.

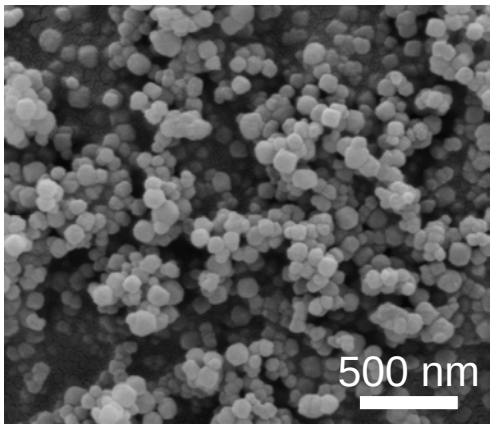

Figure S1. SEM image of UiO-66.

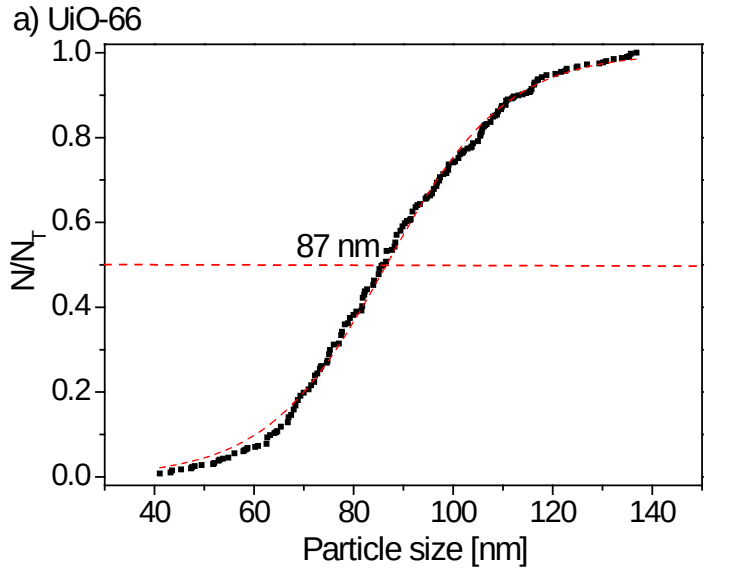
a) UiO-66
1.0
0.8
0.6
0.4
0.2
0.0
N/N_T
87 nm
40
60
80
100
120
140
Particle size [nm]

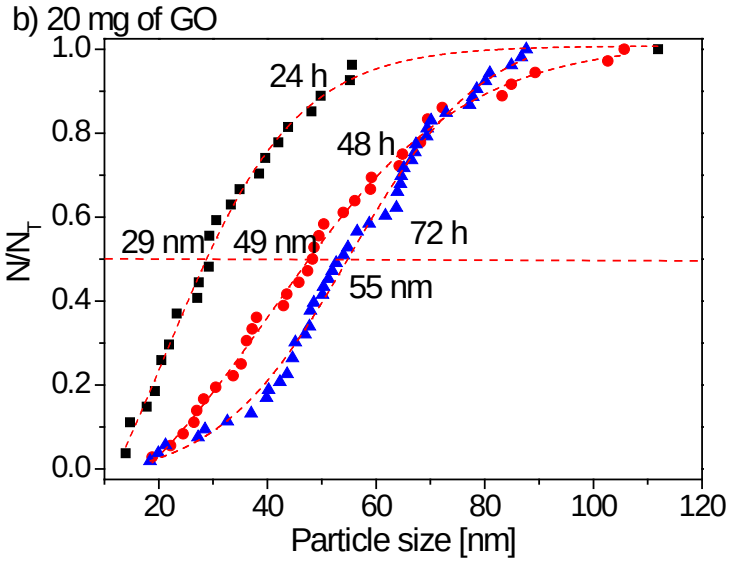
b) 20 mg of GO
1.0
0.8
0.6
0.4
0.2
0.0
N/N_T
24 h
48 h
72 h
29 nm
49 nm
55 nm
20
40
60
80
100
120
Particle size [nm]

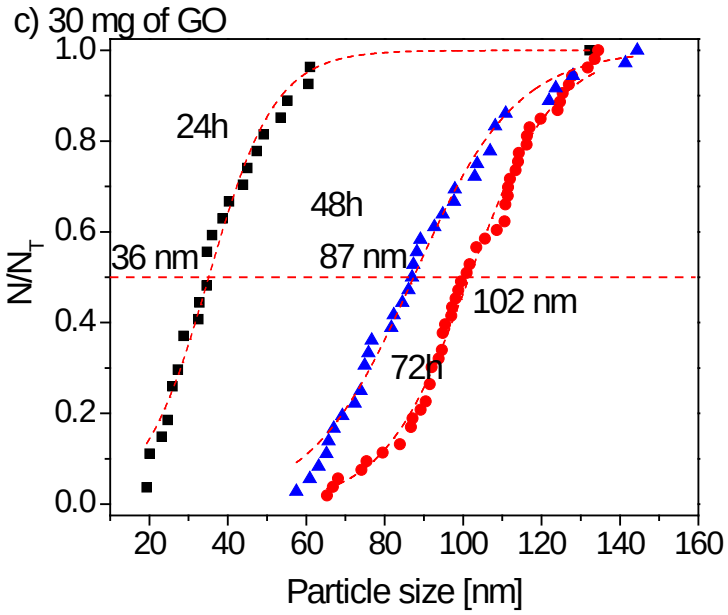

Figure S2. Cumulative distributions of particle size depending on the synthesis time and the amount of GO: a) UiO-66 (0 mg of GO), b) UiO-GO hybrid (20 mg of GO), and c) UiO-GO hybrid (30 mg of GO).

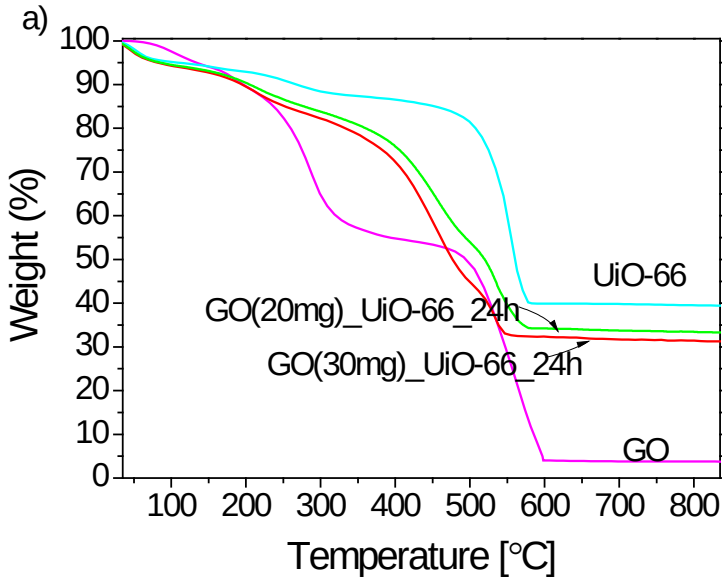

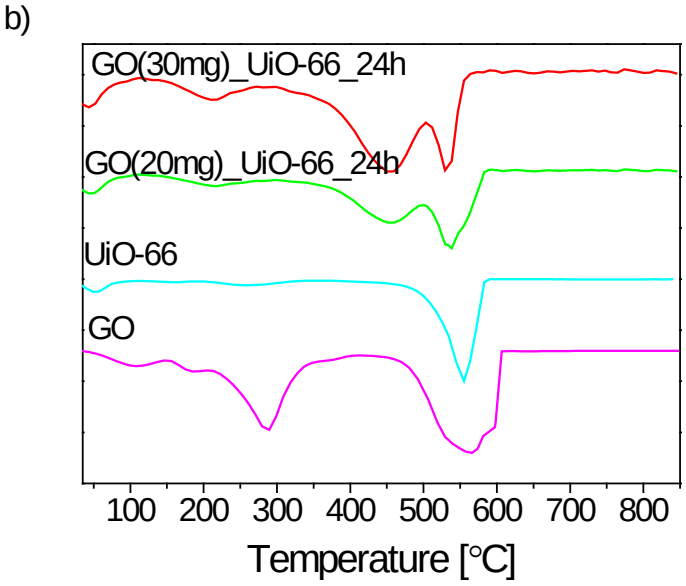

Figure S3. a) TGA curves of GO, UiO-66, GO(20)_UiO-66_24h, GO(30)_UiO-66_24h and b) their derivative curves.

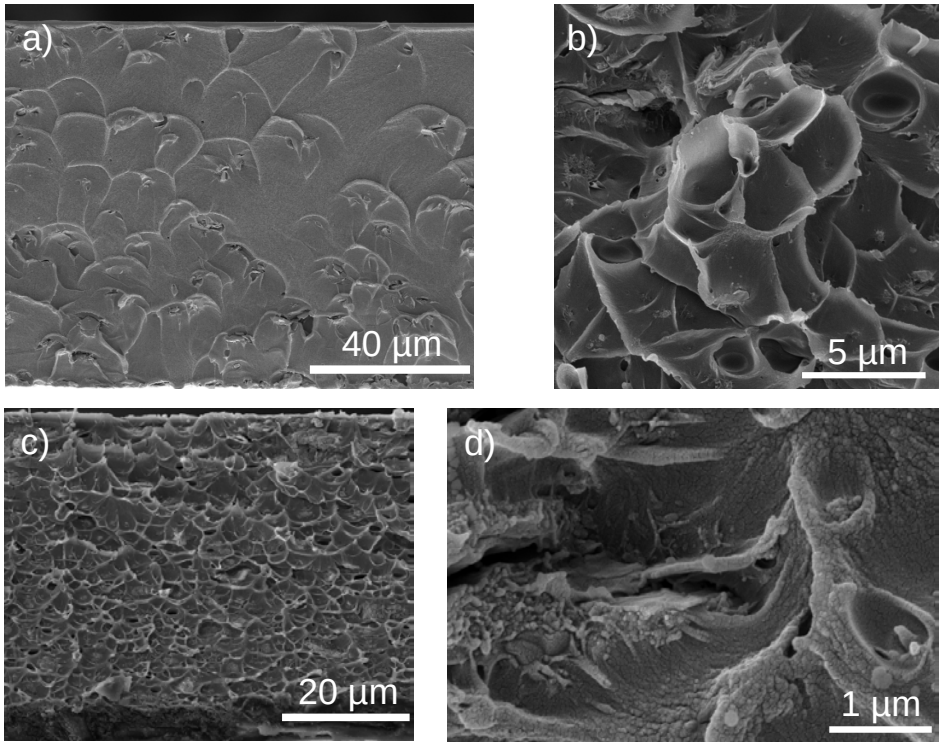

Figure S4. SEM images of cross sections of: a) and b) PI_GO(30)_UiO-66_72h_8; c) and d) PSF_GO(30)_UiO-66_72h_8.

Table S1. Glass Transition temperatures for some of the MMMs prepared.

Membrane	Polymer	Filler [wt%]	T_g [ºC]
Bare PI	PI	-	317 ± 4
PI_GO_8	PI	GO, 8%	320 ± 3
PI_UiO-66_32	PI	UiO-66, 32%	337 ± 3
PI_GO+UiO-66_32	PI	GO+UiO-66, 32%	331 ± 3
PI_GO(30)_UiO-66_48h_32	PI	GO(30)_UiO-66_48h, 32%	336 ± 4
PI_GO(30)_UiO-66_72h_32	PI	GO(30)_UiO-66_72h, 32%	333 ± 3
Bare PSF	PSF	-	183 ± 1
PSF_GO_8	PSF	GO, 8%	187 ± 2
PSF_UiO-66_32	PSF	UiO-66, 32%	195 ± 4
PSF_GO+UiO-66_32	PSF	GO+UiO-66, 32%	191 ± 2
PSF_GO(30)_UiO-66_48h_32	PSF	GO(30)_UiO-66_48h, 32%	195 ± 2
_PSF_GO(30)_UiO-66_72h_32	PSF	GO(30)_UiO-66_72h, 32%	194 ± 2

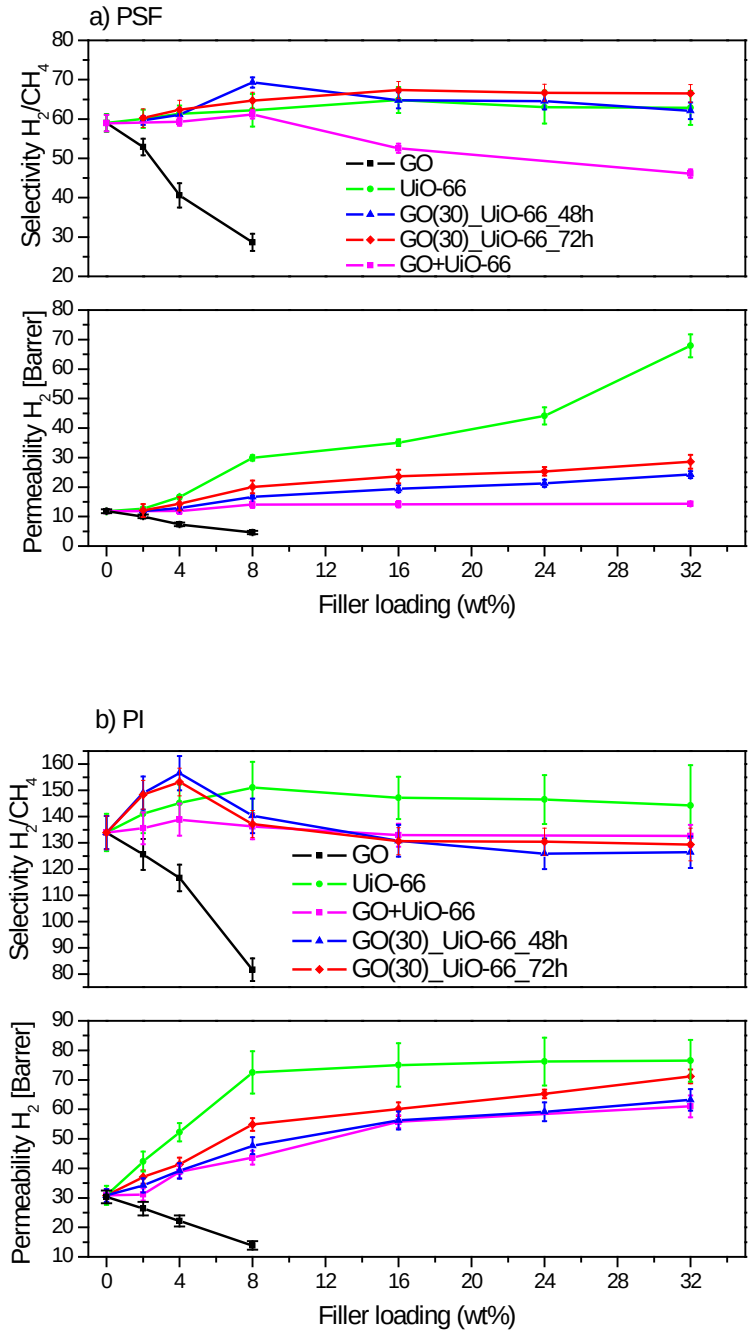

Figure S5. H_2/CH_4 separation results at 35 ºC: a) PSF MMMs and b) PI MMMs.

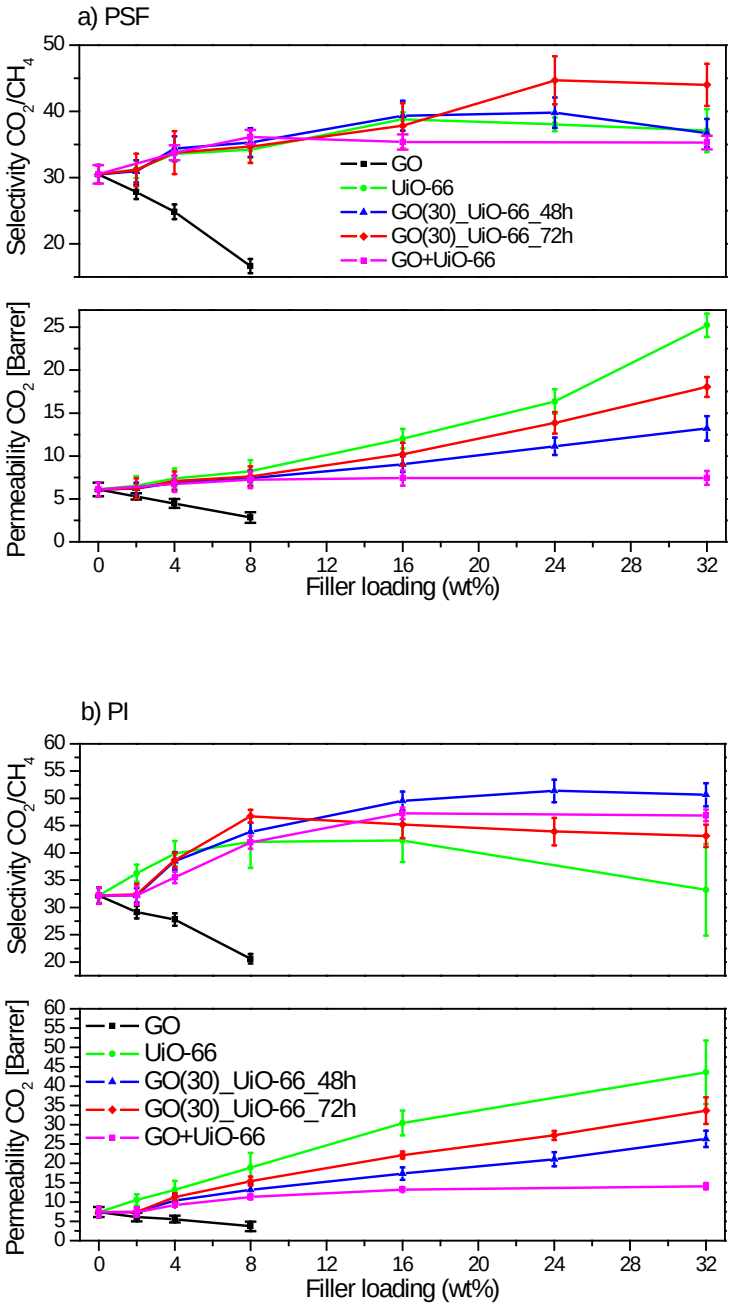

Figure S6. Influence of filler loading on CO_2/CH_4 separation at 35 ºC: a) PSF MMMs and b) PI MMMs.

Table S2. Apparent activation energies of CO_2, CH_4 and H_2 obtained from H_2/CH_4 and CO_2/CH_4 mixtures.

	Apparent activation energy (E_{ap}) [kJ/mol)]			
	Mixture H_2/CH_4		**Mixture CO_2/CH_4**	
Membrane	**H_2**	**CH_4**	**CO_2**	**CH_4**
Bare PSF	14.1	24.7	12.1	27.7
PSF_GO	13.6	24.2	11.8	27.4
PSF_UiO-66	14.8	24.9	12.2	28.1
PSF_GO(30)_UiO-66	14.2	24.9	12.5	28.5
Bare PI	12.2	23.6	12.8	24.7
PI_GO_8	12.1	23.4	12.6	24.4
PI_UiO-66	13.0	24.9	13.7	25.5
PI_GO(30)_UiO-66	12.4	24.0	13.3	25.2